Regular Article

PHYSICAL CHEMISTRY RESEARCH
Published by the
Iranian Chemical Society
www.physchemres.org
info@physchemres.org

Phys. Chem. Res., Vol. 14, No. 1, 227-237, March 2026
DOI: 10.22036/pcr.2025.541290.2725

Structure-Based Design and Identification of Novel Plasmodium Falciparum Falcipain-2 Binders

S. Roy[a], Sh. Bose[b], L. Sarkar[c], P. Pal[d], S. Patra[a], A. Maity[c], H. Verma[e], V. Rathore[e], S. Rajmal Lodha[f], J. Shrivastava[g] and D. Sen[a]*

[a]*Department of Pharmaceutical Chemistry, BCDA College of Pharmacy & Technology, Hridaypur, Kolkata,700127, WB, India*

[b]*Dr. BC Roy College of Pharmacy & AHS, Dr. Meghnad Saha Sarani, Bidhannagar, Durgapur-713212, WB, India*

[c]*Department of Pharmaceutical Technology, JIS University, 81, Nilgunj Road, Agarpara, Kolkata-700109, WB, India*

[d]*Ramkrishna Mahavidyalaya, Kailashahar, 799277, Tripura, India*

[e]*Teerthanker Mahaveer College of Pharmacy, Teerthankar Mahaveer University, Moradabad, UP, 244001, India*

[f]*Department of Pharmaceutical Chemistry, Maliba Pharmacy College, Uka Tarsadia University, Gopal Vidyanagar, Bardoli-Mahuva Road, Tarsadi, Surat, Gujarat,394350, India*

[g]*Department of Pharmacy, School of Health Care and Allied Sciences, G.D Goenka University, Gurugram, Haryana 122103, India*

(Received 14 August 2025, Accepted 11 October 2025)

Malaria remains a significant global health challenge, particularly in developing regions, necessitating the development of novel antimalarial agents. In this study, we employed a combination of structure-based modeling, including molecular docking-based virtual screening, molecular dynamics (MD) simulations, and pharmacokinetic evaluations for identifying potential binders targeting Plasmodium falciparum falcipain-2, a crucial protease for the parasite's survival. A re-docking approach was used to validate the docking protocol, achieving an RMSD of 1.697 Å, indicating high accuracy. The shortlisted compounds were then subjected to MD simulations over 100 ns, where their stability, flexibility, and compactness were analyzed using RMSD, RMSF, and radius of gyration (RoG) metrics. Ligands L2, L3, and L4 exhibited the most promising profiles, demonstrating strong stability, favorable binding orientations, and compatibility with the target's binding site, comparable or superior to the control ligand. Pharmacokinetic properties were assessed, and the drug-likeness of these compounds was confirmed, supporting their potential as falcipain-2 binders. This integrated approach identified promising binders that warrant further *in vitro* and *in vivo* validation for therapeutic application against P. falciparum**.** The methodology and findings contribute valuable insights into structure-based drug design for antimalarial compounds, offering potential approach to combat malaria effectively.

Keywords: Plasmodium falciparum, Falcipain-2, Molecular docking, Virtual screening, Molecular dynamics

INTRODUCTION

Over 200 million cases and almost 600,000 deaths from malaria occur each year, according to the World Health Organization (WHO), making it a danger to world health [1]. More than 90% of deaths from malaria occur in sub-Saharan Africa, where the disease disproportionately affects people, especially pregnant women and children under five [2-5]. *Plasmodium falciparum*, a parasite that infects Anopheles mosquitoes and which people contract through bites, is the main cause of severe malaria cases [6]. Malaria is still common in many areas despite intense global efforts; these conditions are made worse by socioeconomic hardships, poor access to treatment, and mosquito-breeding climate conditions [5-8]. Most of the malaria treatments that are currently available are artemisinin-based combination therapies (ACTs), which combine artemisinin derivatives with a partner medication like lumefantrine or piperaquine

*Corresponding author. E-mail: debanjansen48@gmail.com

[9,10]. While ACTs remain effective in many regions, artemisinin resistance has been observed [11]. The resistance has manifested through delayed parasite clearance times, which pose a significant risk to the efficacy of ACTs [10,12]. The limitations of existing malaria treatments are multifaceted [13-15]. Drug resistance is perhaps the most severe [16], with *P. falciparum* developing resistance to nearly all antimalarial drugs at some point [17,18]. The cost of ACTs and other effective treatments remains prohibitive for many people in low-income regions, limiting accessibility and leading to substandard treatment practices [19-21]. Additionally, some antimalarial drugs, such as Chloroquine, can cause adverse side effects [22], including gastrointestinal disturbances, visual disturbances, and, in rare cases, severe neuropsychiatric symptoms. These challenges emphasize the need for new antimalarials that are cost-effective, safe, and efficacious against resistant strains of *P. falciparum* [12,23]. In the search for new antimalarial agents, research has predominantly focused on a limited set of drug targets within the parasite [14,19,24,25]. Current targets include heme detoxification, protein synthesis, and nucleic acid synthesis pathways [26-28]. However, *P. falciparum* possesses unique proteases essential for its survival, presenting underexplored opportunities for drug development [29]. Cysteine proteases, such as falcipains [30], play a critical role in the parasite's lifecycle, particularly during the erythrocytic stage when the parasite breaks down host hemoglobin to acquire amino acids [31,32]. Among these, falcipain-2 is particularly essential [33], as it facilitates hemoglobin digestion and is integral to parasite survival and proliferation [34]. The selection of compounds with desirable drug-like properties is aided by computations and ADME (Absorption, Distribution, Metabolism, and Excretion) features. In this investigation, we used CADD to find putative falcipain-2 binders. We began with a verified pharmacophore model and used an internal phase database to find drugs that met the necessary pharmacophoric characteristics for binding falcipain-2. The compounds underwent molecular docking following identification to assess their interactions and binding affinities with falcipain-2. The stability of the ligand-protein complexes under physiological settings was then evaluated using molecular dynamics simulations. To enhance our selection process, we conducted MMGBSA computations to approximate the binding free energies and assessed ADME attributes to verify drug-like features. We hope to find promising leads for the development of this thorough methodology.

MATERIAL AND METHODS

Using an Intel i7-9700K processor with 32 GB of RAM and an NVIDIA RTX 2070 GPU, Linux Mint 21.1 was used to run all computational tasks for this investigation. The free Maestro of Schrodinger LLC (under academic licence), Visual Molecular Dynamics (VMD) [35], and PyMOL [36] were used to visualize molecular structures, exploring interactions and rendering images. DataWarrior (https://openmolecules.org/datawarrior/) was used to handle, retrieve, and compute physicochemical properties. For graphical representation, Grace software (https://plasma-gate.weizmann.ac.il/Grace/) was employed as the primary plotting tool.

Data Collection

A total of 30 P. falciparum falcipain-2 inhibitors, each with IC_{50} values in the nanomolar range, were retrieved from the ChEMBL database and utilized in this study. The X-ray crystal structure of P. falciparum falcipain-2 (PDB ID: 6SSZ) was obtained from the Protein Data Bank [37].

Protein Preparation

The crystal structure of the protein was retrieved from the ProteinDataBank, providing valuable insights into the intricate details of P. falciparum falcipain-2 at an impressive resolution of 3.45 Å. Energy minimization is a critical step in protein modeling, as it reduces net interatomic forces to achieve a stable conformation. Consequently, optimizing the protein structure is essential for structure-based drug design (SBDD). Using the PrepWizard module of Maestro from Schrodinger LLC (under academic license), the protein structure was refined to its optimal state, utilizing the OPLS3E force field [39] at a pH of 7.2. Hydrogen atoms were added, and heteroatoms such as water molecules and ions were removed. Chain A was selected for the study, as the crystal structure comprises a heterodimer containing chains A and B. A Ramachandran plot was employed to validate the protein structure.

Ligand Preparation

All ligands (0.7 million) used in this study were prepared using the RDkit library of the Python programming package [38]. The ligands were collected from various databases, such as the Zinc natural product database (https://zinc12.docking.org/browse/catalogs/natural-products), Mcule (https://mcule.com/database/), NPASS (https://bidd.group/NPASS), and Enamine database (https://enamine.net/). The pH was set to 7.2, and the desalt option was applied to prepare the ligands. The GAFF force field was utilized, and 10,000 conformers were generated. Low-energy conformations were stored for further analysis, followed by energy minimization.

Validation of Docking Protocol and Virtual Screening

The molecular docking protocol was validated using a re-docking approach. The co-crystalized ligand was extracted from the protein-ligand complex and redrawn [40]. Following subsequent preparation, the ligand was docked into the defined ligand binding site of the receptor (receptor grid coordinates: X, Y, Z = 17, -40, 5.04). A total of 50 poses were generated, and each pose was superimposed on the native pose of the ligand to calculate the root mean square deviation (RMSD). The prepared molecules were subjected to molecular docking studies based on virtual screening utilizing Vina 1.2. An in-house bash script was utilized to execute the virtual screening experiments [41].

Molecular Dynamics (MD)

The MD simulations were executed using AMBER 24 (Assisted Model Building with Energy Refinement) integrated with AMBER Tools 2024 [42]. The Antichember module was utilized to parameterize the ligands, while the GAFF2 force field was applied. The pdb4amber module, associated with the tleap module of Amber Tools, was used for protein parameterization, followed by the incorporation of the protein-ligand complex into a cubic water box of dimensions 10 Å × 10 Å × 10 Å. The ff14SB force field was employed for protein parameterization, and the TIP3P water model was used for the preparation of each system. Additionally, 1.5 M KCl was added to each system subjected for the simulation setup. After minimization, an *NVT* (where the number of particles is denoted by N, the system volume (V), and the temperature T) and *NPT* (where the number of particles is represented by N, the system pressure denoted by P, and temperature T) ensemble 100ns molecular dynamics simulation was conducted for each system, including the Apo protein. For the MD simulations, a cut-off distance of 8.0 Å (0.8 nm) was applied for short-range non-bonded interactions, including van der Waals and Coulombic interactions. Detailed protocols for these procedures can be found in our previously published work [42].

Molecular Mechanics Generalized Born Surface Area (MMGBSA)

The MM-GBSA calculations were performed using the MMPBSA.py.MPI module of AMBER Tools. Every 10^{th} frame was extracted from the 100 ns molecular dynamics trajectory and subjected to thermodynamic data calculations.

Absorption, Distribution, Metabolism, and Excretion (ADME) Properties Calculation

The pharmacokinetic profiles of each ligand were calculated using the SwissADME web server tool [43]. The SMILES representation of each ligand was supplied as input. The results of the ADME calculations were recorded manually. Additionally, the drug-likeness properties of each ligand were assessed using the DataWarrior tool.

RESULTS AND DISCUSSION

A combination of structure-based virtual screening and molecular dynamics simulations was performed. For successful structure-based design, validating the protein structure poses significant importance. The Ramachandran plot constructed for the prepared protein structure is presented in Supplementary Fig. 1 (SF-1). The plot clearly demonstrates that all residues lie within the allowed regions, indicating the acceptability of the protein structure. To validate the docking protocol, a re-docking approach was employed. After superimposing the best docking pose onto its native pose (Fig. 1), the root mean square deviation (RMSD) was calculated to be 1.697 Å with the corresponding docking score -3.768 kJ mol^{-1}. A value of -5.0 kJ mol^{-1} was selected as the threshold of the docking score.

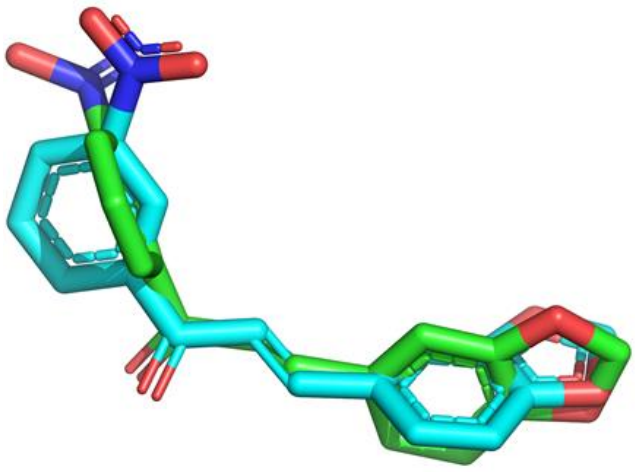

Fig. 1. Superimposition of Docked pose (Cyan) upon native pose (Green).

A molecule will be retained if it depicts a docking score less than -5.0 kJ mol^{-1}. The RMSD value indicates that the docking protocol can be accepted for virtual screening [40].

A total of 0.7 million molecules from various databases were subjected to three stages of virtual screening experiments. The top 20% of the output from the first stage of docking, known as high-throughput virtual screening (HTVS), was then subjected to the second stage, which involved standard precision docking (SP). The top 15% of the output from the SP docking was further evaluated using extra precision (XP) docking. Initially, the docking score was considered for shortlisting the ligands. Subsequently, the binding orientation within the receptor pocket and the residue interaction profile were analyzed to select the final top five ligands. The summarised results of docking experiments can be found in Table 1.

Table 1. Results of Docking Experiments

SL No.	Ligand name	Zinc id	Docking score	H-BOND	Hydrophobic	Others
1	Control ligand	--	-3.768	ASN A:21	ALA A:25,ALA A:140,TRP A 193,TRP A: 189,CYS A 22	TRP A:189 π-π cation
2	L3	ZINC000005220456	-5.562	CYS A:22,GLN A:19,	CYS A:22,ALA A:25,VAL A:135,TRP A:193,TRP A:189,ALA A:140,CYS A:63,	HIE A:157,ASN A:156,ASN A:64,GLN A:19,LYS A:20
3	L2	ZINC000004200852	-5.691	GLN A:19,ASN A:21,ASN A 156,HIE A157	CYS A:63,TRP A:189,TRP A:193,ALA A;140,ALA A:25,CYS A:22,VAL A:135	GLN A:19,LYS A:20,ASN A:21,SER A:136,HIE A:157,ASN A:156,GLY A:65,GLY A:66
4	L3	ZINC000012883066	-6.099	GLN A:19,CYS A:22,ALA A:25,ASN A:156,	TRP A:189,ALA A:140,CYS A:63,ALA A:25,CYS A:22,VAL A:135	HIE A:157,ASN A:156,ASN A:64,GLY A 65,SER A;24,GLY A:23,ASN A:21,LYS A:20,GLN A:19 ASP A:18
5	L4	ZINC000004102491	-6.107	GLN A:19,ASN A:21,HIE A:157,ASN A:156	CYS A:22,TRP A:189,ALA A:140,VAL A:135,CYS A:63,TRP A:193	LYS A:20,ASN A:21,GLN A:19,ASP A:18,HIE A:157,ASN A:156,ASN A:64GLY A:23
6	L5	ZINC000008643826	-6.854	CYS A:22,ASN A:21,ASN A:156	ALA A:25,CYS A:22,ALA A:140,TRP A:189,TRP A:193,VAL A:135	GLY A:65,GLY A:23,ASN A:21,LYS A:20,GLN A:19,GLN A:192,HIE A:157,ASN A:156
7	L6	ZINC000031159786	-6.854	GLN A:19,ASN A:21,TRP A:189,HIE A:157,GLY A:66	CYS A:22,VAL A:135,TRP A:26,ALA A:158,TRP A:189,TRP A:193	ASP A:18, GLN A:19, LYS A:20, ASN A:21, ASN A:156, HIE A:157, GLY A:66, GLY A:66,GLY A:23

We visually investigate the binding interactions of several ligands with the active site of *P. falciparum* falcipain-2 through molecular docking. Results of the top six ligands with their docking scores, hydrogen bond interactions, and hydrophobic interactions are listed in Table 1. The control ligand exhibited a docking score of -3.768 kJ mol^{-1}, while the identified ligands displayed significantly improved binding affinities, indicating their potential as effective binders. Among the ligands tested, L5 (ZINC000008643826) and L6 (ZINC000031159786) demonstrated the highest docking scores of -6.854 kJ mol^{-1}, indicating strong binding affinity towards the active site of *P. falciparum* falcipain-2.

These scores are substantially lower than the control ligand, underscoring the potential of these identified ligands for further investigation. Docking scores of the remaining ligands showed a similar trend of increased binding efficiency, ranging from -5.562 kJ mol^{-1} (L3) to -6.107 kJ mol^{-1} (L4). The ligand-receptor combination is stabilized primarily by the hydrogen bond interactions (Fig. 2). The strong binding affinity of all discovered ligands was attributed to the formation of substantial hydrogen bonds with essential residues in the active site. As an illustration of a strong binding profile, L5 formed contacts with CYS A:22, ASN A:21, and ASN A:156. Likewise, L6 established hydrogen bonds with residues that are essential for preserving the protein-ligand complex's structural integrity, including GLN A:19, ASN A:21, and TRP A:189. In addition, hydrophobic interactions are essential for ligand binding.

The ligands that were found had advantageous hydrophobic interactions with several residues in the binding. A comparison study was conducted using the co-crystallized ligand. In comparison to the discovered ligands, the control ligand had a docking score of -3.768 kJ mol^{-1} and generated fewer hydrogen bonds. As an example, the co-crystallized ligand was stabilized mainly by a small number of interactions inside the binding pocket, while the identified ligands showed larger hydrophobic contacts and hydrogen bond networks in addition to lower docking scores. Additionally, L2 (ZINC000004200852) and L3 (ZINC000005220456) showed encouraging interactions, with respective docking scores of -5.691 kJ mol^{-1} and -5.562 kJ mol^{-1}. Their capacity to form many hydrogen bonds and hydrophobic contact points to their potential for use as P. falciparum falcipain-2 competitive inhibitors. This pattern was also supported by L4 (ZINC000004102491) and L5, both of which had docking scores more than -6.1 kJ mol^{-1}.

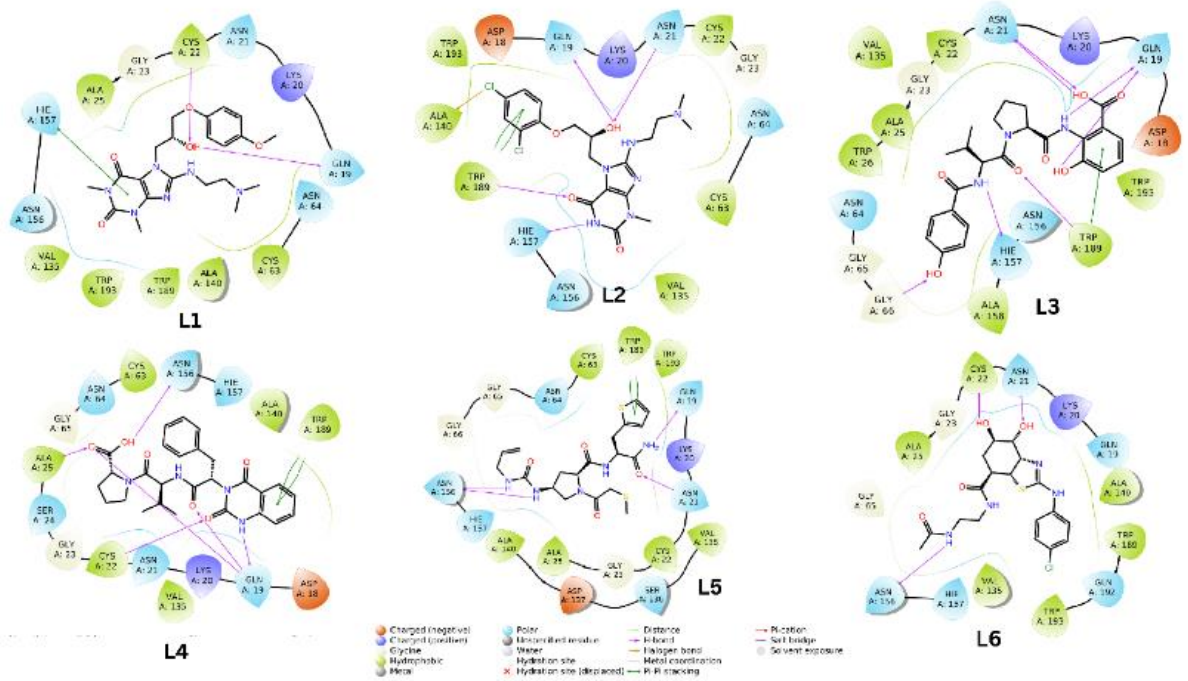

Fig. 2. Protein Ligand 2D interaction diagram of the top six ligands.

100ns MD simulations under *NVT* and *NPT* ensembles for each ligand-bound system were conducted to assess the stability of the protein-ligand complexes. Furthermore, MD simulations were performed for the control ligand (co-crystallized ligand) complex and the apoprotein. To evaluate the stability and dynamics of the systems, the root mean square deviation (RMSD), root mean square fluctuation (RMSF), and radius of gyration (RoG) were computed from the MD trajectories. The overall stability of the protein-ligand complexes during the simulation can be inferred from the RMSD values. A steady RMSD value means that the interactions between the ligand and protein remain constant across time. The simulation's individual residues' flexibility is demonstrated by the RMSF values. High RMSF values suggest more adaptability. Figure 3 shows a graphical representation of the MD results. The summary of the results of the molecular dynamics experiments is presented in Table 2.

The range of the apo protein's RMSD was 0.47 Å to 2.41 Å, with an average of 1.54 Å. This indicates a moderate degree of stability with some structural variability, which is best represented by the upper limit of the RMSD. The average RMSD of the control ligand (co-crystallized ligand) complex was 2.06 Å, higher than the apo protein. The range showed a wider fluctuation range, ranging from 0.51 Å to 2.86 Å. This suggests that even if the control ligand attaches to the protein, there could have been more conformational changes in the complex throughout the simulation. The typical RMSD values of L1, L3, and L4 ligands were comparatively low, with L1 measuring 1.49 Å and L3 measuring 1.57 Å.

The L6 displayed the largest RMSD at 2.72 Å, indicating a comparatively higher flexibility level. Similar average RMSD values were observed for the apoprotein and L1–L4, suggesting that the structural integrity of these ligands is maintained at a level similar to that of the unbound protein.

Table 2. Results of Molecular Dynamics Experiments

SL NO		RMSD (Å) (Backbone) 100ns			RMSF (Å) (Backbone) 100ns			Rg (Å) (Backbone) 100ns			MMGBSA
		AVG	MIN	MAX	AVG	MIN	MAX	AVG	MIN	MAX	
1	Apo	1.54	0.47	2.41	7.91	1.16	17.92	18.34	18.005	18.74	--
2	CL	2.06	0.51	2.86	10.78	1.45	28.11	18.48	18.09	18.93	-15±1.2
3	L1	1.49	0.51	2.27	10.52	1.18	20.99	18.31	17.94	18.63	-26±1.1
4	L2	1.75	0.55	2.58	9.22	1.50	17.42	18.27	17.85	18.71	-32±1.4
5	L3	1.57	0.52	2.5	8.77	1.17	16.5	18.31	17.90	18.78	-21±1.1
6	L4	1.55	0.5	2.35	9.68	1.35	19.84	18.23	17.85	18.60	-24±1.3
7	L5	1.6	0.45	2.63	8.80	1.39	18.65	18.27	17.87	18.67	-40±1.4
8	L6	1.8	0.54	2.72	8.91	1.25	17.44	18.36	18.02	18.76	-23±1.4

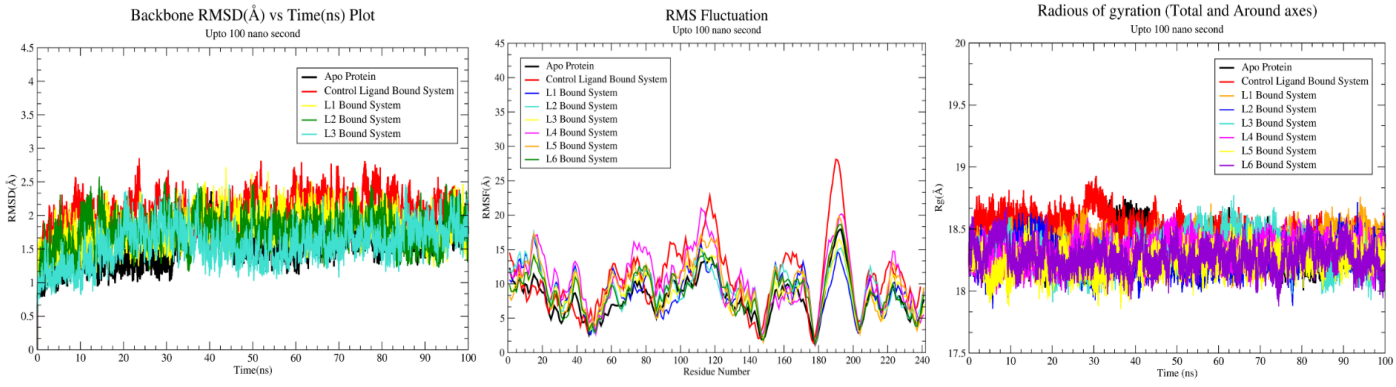

Fig. 3. Graphical representation of MD simulation results.

The average RMSD values of L2, L5, and L6 were higher and more in line with the control ligand system. This implies that these ligands modify the conformation to some extent, possibly as a result of an enhanced fit or flexibility in the binding pocket. With minimal disruption to the protein's structure and low average and maximum RMSD values below 2.5 Å, L1 and L3 exhibited the most advantageous profiles. This suggests that they offer a stable binding relationship. The apo protein showed variations in its average RMSF of 7.91 Å. The average RMSF of 10.78L4 and L6 was greater for the control ligand complex. While L4 showed a somewhat greater maximum RMSF of 19.84 Å, with a broader range from 1.45 Å to 28.11 Å, these ligands demonstrated flexibility levels similar to L1, with average RMSF values of 9.68 Å and 8.91 Å, respectively. Thus, compared to the apo protein, the control ligand complex had greater residue flexibility, suggesting that certain areas of the protein structure may be able to adjust to ligand binding.L1: Although L1 preserved overall stability, it permitted certain flexible zones, as seen by the average RMSF of 10.52 Å, which ranged from a minimum of 1.18 Å to a maximum of 20.99 Å. Comparing these ligands to the control ligand, L2, L3, and L5 showed comparatively reduced average RMSF values, with L2demonstrating a somewhat moderate degree of flexibility.L4 and L6: These ligands showed flexibility levels comparable to L1, with average RMSF values of 9.68 Å and 8.91 Å, respectively. However, L4 had a marginally higher maximum RMSF of 19.84 Å. Profiles of Flexibility: In comparison to the control ligand, ligands L2, L3, L5, and L6 showed decreased average and maximum RMSF values. This implies that they minimized significant oscillations by giving the protein more structural stability. The most flexible ligand complex was the control one, most likely because of its interaction with a flexible binding pocket or other conformational changes that were caused. The greatly reduced flexibility of ligands L3 and L5 raises the possibility that they are part of a more rigid and stable protein-ligand complex. With the protein stabilizing effect of L3, which has the lowest maximum RMSF value of 16.5 Å. The average RoG of the control ligand complex was slightly higher, 18.48 Å, with a range of 18.09 Å to 18.93 Å. The observed rise in RoG in relation to the apo protein implies a marginal enlargement of the protein's structure upon ligand binding, potentially signifying induced conformational modifications or a minor relaxation of the protein structure. The L1: The protein's overall compactness was preserved in a manner akin to the apo state, as seen by the low departure from the apo protein, with an average RoG of 18.31 Å. L2 and L4: With averages of 18.27 Å and 18.23 Å, respectively, both L2 and L4 showed RoG values that were comparable to the apo protein. Additionally, their ranges were similar, suggesting that these ligands kept the protein's compact structure intact during the simulation. L3: Displaying. The RoG values of the ligand-bound systems were similar to those of the apo protein, suggesting that the compactness of the protein was not substantially changed by the addition of ligands. On average, the control ligand exhibited a somewhat greater RoG, indicating a little relaxation of the protein structure. L4 showed the lowest average RoG of all the ligands examined, suggesting a somewhat more compact structure and maybe improved stability and decreased conformational fluctuations. Conversely, L3 and L1 maintained compactness similar to the apo state, supporting their stabilizing potential. The Control Ligand has a modest binding affinity with a binding free energy of -15 ± 1.2 kcal mol^{-1}. From L1 to L6, ligands L2 and L5 exhibit the best binding free energies (L2: -32 ± 1.4 kcal mol^{-1}, L5: -40 ± 1.4 kcal mol^{-1}), indicating robust protein binding. When compared to the control ligand, L1 (-26 ± 1.1 kcal mol^{-1}) and L4 (-24 ± 1.3 kcal mol^{-1}) similarly exhibit good binding affinities, while L6 (-23 ± 1.4 kcal mol^{-1}) and L3 (-21 ± 1.1 kcal mol^{-1}) show marginally weaker but still promising interactions.

All six ligands (L1 to L6) are analysed in this study according to their ADME (Absorption, Distribution, Metabolism, and Excretion) characteristics (Table 3).

These factors are essential for assessing the compounds' probable pharmacokinetic behavior and drug-likeness. To determine whether they are suitable for further development, key features such as molecular weight, cLogP (lipophilicity), cLogS (solubility), hydrogen bond acceptors and donors, topological polar surface area (TPSA), and drug-likeness are compared. The ligands have molecular weights between 426.11 g mol^{-1} (L4) and 506.22 g mol^{-1} (L5). L4 is the most advantageous ligand since it has a molecular weight of less than 500 g mol^{-1}, which is normally preferable for oral bioavailability; L5 just touches the threshold. Hydrophobicity is measured by cLogP, with

Table 3. ADME Properties

Molecule	Mol.weight	cLogP	cLogS	H-Acceptors	H-Donors	TPSA
ZINC000004102491	470.12	180.3931632347	2.27436501876772	10	3	117.41
ZINC000004200852	453.15	174.454684902841	1.10740050178988	9	5	133.63
ZINC000005220456	446.23	136.304498548749	1.72728431532644	11	2	115.78
ZINC000008643826	426.11	176.987942072561	2.38089208800686	8	5	123.05
ZINC000012883066	506.22	193.921911717095	1.71006452972814	10	3	141.57
ZINC000031159786	469.18	206.592319910416	1.38330438701871	10	5	156.27

values between 1 and 5 being optimal for substances that resemble drugs. Every ligand shows much higher values, indicating a high degree of lipophilicity that may impede absorption and solubility. L6 and L5 had the highest cLogP values (206.59 and 193.92, respectively), indicating that both are quite lipophilic and may provide concerns for bioavailability. Even while L3's cLogP (136.30) is the lowest, it is still over the ideal range, suggesting that there may be some solubility issues. Higher values of the cLogS parameter indicate better solubility in water. It predicts aqueous solubility. With the greatest cLogS (2.27), the L1 appears to be more soluble than the others. With the lowest cLogS (1.38), L6 has poor solubility, which may have an impact on distribution and absorption in biological systems. L2 follows suit with a cLogS of 1.12. There are 8 (L4) to 11 (L3) hydrogen bond acceptors in total. The number of donors of hydrogen bonds is 2 (L3) to 5 (L2 and L6). Stronger interactions with biological targets are frequently correlated with increased numbers of donors and acceptors. The greatest number of donors (5) is shared by L2 and L6, which may improve their protein-binding affinity. •The compound's TPSA values show how well it penetrates membranes. In general, values below 140 Å² are advantageous for good permeability. With a TPSA of 123.05 Å², L4 is a good choice for permeability in membranes. The fact that L6 (156.27 Å²) and L5 (141.57 Å²) are above the threshold may suggest that they have issues bridging biological membranes. Drug-likeness is a composite score that indicates a molecule's overall likelihood for success as a therapeutic candidate. Higher numbers are ideal. With the greatest drug-likeness score (7.34), L1 appears to be the most promising candidate for additional research and development. With a score of 3.52, L5 has the lowest overall drug-likeness profile; this could be because of its poor solubility and larger molecular weight. With adequate ADME characteristics, high solubility, and drug-likeness, L1 is the most well-rounded contender. L2 has reasonable permeability and drug-likeness; however, its reduced solubility may present concerns. L3 has an adequate TPSA and a moderate drug-likeness, although there may be issues due to its limited solubility. L4 has a well-balanced profile with good potential for bioavailability and permeability, but its high lipophilicity may prevent it from being absorbed fully. L5 is the least promising for development due to its low membrane permeability, high lipophilicity, and lowest drug-likeness. Even while L6 is superior to L5, its high TPSA and poor solubility limit its potential as a therapeutic candidate. Based on ADME and MD studies, L1 is clearly the best contender, with L2, L3, and L4 being the next best choices. Without additional structural alteration, L5 and L6 are less suited due to notable limits in their pharmacokinetic profiles and stability in molecular dynamics. Based on the above analyses, it can be stated that ligands L1, L2, L3, and L4 demonstrated the best overall profiles across RMSD, RMSF, and RoG, indicating favourable stability, moderate flexibility, and maintained compactness in complex with the protein. L1 showed slightly higher flexibility, similar to the control ligand, but maintained an overall stable structure. The results highlight L1 to L4 as particularly promising candidates, with L2 also showing strong stability, making these ligands ideal for further study as potential binders of P. falciparum falcipain-2.

CONCLUSION

Molecular docking, molecular dynamics (MD) simulations, pharmacokinetic analyses, and structure-based pharmacophore modeling were used to analyze the binding

potential of ligands L1 to L6 with P. falciparum falcipain-2. With docking scores of -6.854 kJ mol^{-1}, ligands L5 (ZINC000008643826) and L6 (ZINC000031159786) showed the greatest binding affinities, surpassing the performance of the control ligand (-3.768 kJ mol^{-1}). L5 engaged with CYS A:22, ASN A:21, and ASN A:156, whereas L6 made bonds with GLN A:19, ASN A:21, and TRP A:189. Both L5 and L6 produced important hydrogen bonds with crucial residues. Strong docking scores and stable complexes were also demonstrated by ligands L2 (ZINC000004200852), L3 (ZINC000005220456), and L4 (ZINC000004102491). L3 had the least flexibility in RMSF values. With low RMSD values (below 1.57 Å), MD simulations verified the stability of L1, L3, and L4, but L6 showed greater flexibility (RMSD 2.72 Å). The results of the binding affinity were confirmed by the MMGBSA free energy analysis, where L5 had the highest binding free energy (-40 ± 1.4 kcal mol^{-1}) and L2 had the second-highest (-32 ± 1.4 kcal mol^{-1}). L1's persistent association with the protein was further supported by its significant binding energy of -26 ± 1.1 kcal mol^{-1}. With a balanced binding affinity, stability, excellent ADME profile, high drug-likeness (7.34), and good solubility, L1 stood up as the best overall candidate. Additionally, L2, L3, and L4 showed encouraging stability and binding potential. L5 and L6 exhibited strong binding affinities; however, structural optimization is required due to their high lipophilicity, low solubility, and decreased stability in MD simulations. L1 to L4 are the most promising binders of P. falciparum falcipain-2, with L1 upended out as the lead candidate for further investigation.

ACKNOWLEDGEMENT

S Kar thanks to ken University for providing necessary facilities like software licences.

REFERENCES

[1] Buck, E.; Finnigan, N. A., *Malaria*. In StatPearls [Internet]. StatPearls **2025**, Publishing. https://www.ncbi.nlm.nih.gov/books/NBK551711.

[2] Bhatt, S.; Weiss, D. J.; Cameron, E.; Bisanzio, D.; Mappin, B.; Dalrymple, U.; Battle, K.; Moyes, C. L.; Henry, A.; Eckhoff, P. A.; Wenger, E. A.; Briët, O.; Penny, M. A.; Smith, T. A.; Bennett, A.; Yukich, J.; Eisele, T. P.; Griffin, J. T.; Fergus, C. A.; Lynch, M.; Lindgren, F.; Cohen, J. M.; Murray, C. L. J.; Smith, D. L.; Hay, S. I.; Cibulskis, R. E.; Gething, P. W., The effect of malaria control on *Plasmodium falciparum* in Africa between 2000 and 2015. *Nature*, **2015**, *526*(7572), 207-211. https://doi.org/10.1038/nature15535.

[3] Duffey, M.; Shafer, R. W.; Timm, J.; Burrows, J. N.; Fotouhi, N.; Cockett, M.; Leroy, D., Combating antimicrobial resistance in malaria, HIV and tuberculosis. *Nature Reviews Drug Discovery*, **2024**, *23*(6), 461-479. https://doi.org/10.1038/s41573-024-00933-4.

[4] Li, J.; Docile, H. J.; Fisher, D.; Pronyuk, K.; Zhao, L., Current status of malaria control and elimination in Africa: Epidemiology, diagnosis, treatment, progress and challenges. *Journal of Epidemiology and Global Health*, **2024**, *14*(3), 561-579. https://doi.org/10.1007/s44197-024-00228-2.

[5] Lu, F., Biological threats to global malaria elimination: Antimalarial drug resistance [in Chinese]. *Zhongguo Xue Xi Chong Bing Fang Zhi Za Zhi*, **2024**, *36*(3), 233-238. https://doi.org/10.16250/j.32.1374.2024091.

[6] Snow, R. W.; Guerra, C. A.; Noor, A. M.; Myint, H. Y.; Hay, S. I., The global distribution of clinical episodes of *Plasmodium falciparum* malaria. *Nature*, **2005**, *434*(7030), 214-217. https://doi.org/10.1038/nature03342.

[7] Vythilingam, I.; Jeyaprakasam, N. K., Deforestation and non-human primate malarias will be a threat to malaria elimination in the future: Insights from Southeast Asia. *Acta Tropica*, **2024**, *257*, 107280. https://doi.org/10.1016/j.actatropica.2024.107280.

[8] Zekar, L.; Sharman, T., *Plasmodium falciparum malaria*. In StatPearls. **2023**, StatPearls Publishing. https://www.ncbi.nlm.nih.gov/books/NBK551784/

[9] Kumari, A.; Singh, S.; Gupta, P.; Kumar, R.; Singh, P., Synthesis, molecular docking and dynamics study of novel epoxide derivatives of 1,2,4-trioxanes as antimalarial agents. *Structural Chemistry*, **2022**, *33*(3), 907-919. https://doi.org/10.1007/s11224-022-01885-4.

[10] Meshnick, S. R., Artemisinin antimalarials: Mechanisms of action and resistance. *Médecine Tropicale*, **1998**, *58*(3 Suppl), 13-17.

[11] White, N. J.; Chotivanich, K., Artemisinin-resistant malaria. Clinical Microbiology Reviews, **2024**, e0010924. DOI: 10.1128/cmr.00109-24.

[12] Sen, D.; Chatterjee, T. K., Pharmacophore modeling and 3D quantitative structure-activity relationship analysis of febrifugine analogues as potent antimalarial agents. *Journal of Advanced Pharmaceutical Technology & Research*, **2013**, *4*(1), 50-60. DOI: 10.4103/2231-4040.107501.

[13] Goodwin, J.; Arinaitwe, E.; Nankabirwa, J. I.; Rek, J. C.; Bousema, T.; Drakeley, C.; ... & Conrad, M. D., Persistent and multiclonal malaria parasite dynamics despite extended artemether-lumefantrine treatment in children. *Nature Communications*, **2024**, *15*(1), 3817. DOI: 10.1038/s41467-024-48210-7.

[14]Okombo, J., & Fidock, D. A. Towards next-generation treatment options to combat Plasmodium falciparum malaria. *Nature Reviews Microbiology*. **2024**, *23*(3), 178-191. DOI: 10.1038/s41579-024-01099-x.

[15] van Schalkwyk, D. A.; Sutherland, C. J.; Schwimmer, J. B.; Owens, C.; Dodoo, A.; Roper, C.; & Burza, S.. Treatment failure in a UK malaria patient harboring genetically variant *Plasmodium falciparum* from Uganda with reduced in vitro susceptibility to artemisinin and lumefantrine. *Clinical Infectious Diseases*, **2024**, *78*(2), 445-452. https://doi.org/10.1093/cid/ciad724

[16] Sinha, S.; Medhi, B.; Sehgal, R., Challenges of drug-resistant malaria. *Parasite*, **2014**, *21*, 61. DOI: 10.1051/parasite/2014059

[17] Amelo, W.; Makonnen, E., Efforts made to eliminate drug-resistant malaria and its challenges. *BioMed Research International*, **2021**, 5539544. DOI: 10.1155/2021/5539544.

[18] Hyde, J. E., Drug-resistant malaria. *Trends in Parasitology*, **2005**, *21*(11), 494-498. DOI: 10.1016/j.pt.2005.08.020.

[19] Achan, J.; Barry, A.; Leroy, D.; Kamara, G.; Duparc, S.; Kaszubska, W.; Gandhi, P.; Buffet, B.; Tshilab, P.; Ogutu, B.; Taylor, T.; Krishna, S.; Richardson, N.; Ramachandruni, H.; Rietveld, H., Defining the next generation of severe malaria treatment: A target product profile. *Malaria Journal*, **2024**, *23*(1), 174. https://doi.org/10.1186/s12936-024-04986-z

[20] Kokori, E.; Olatunji, G.; Akinboade, A.; Akinoso, A.; Egbunu, E.; Aremu, S. A.; Okafor, C. E.; Oluwole, O.; Aderinto, N., Triple artemisinin-based combination therapy (TACT): Advancing malaria control and eradication efforts. *Malaria Journal*, **2024**, *23*(1), 25. https://doi.org/10.1186/s12936-024-04844-y

[21] Sinha, S.; Sharma, S.; Singh, K.; Swarnkar, D.; Ahmed, N.; Rajput, P.; Srivastava, B.; Anvikar, A. R., Efficacy and safety of artemisinin combination therapy for the treatment of uncomplicated *Plasmodium falciparum* malaria across international borders of India. *Journal of Vector Borne Diseases*, **2024**, *61*(1), 81-89. https://doi.org/10.4103/0972-9062.392254

[22] Stokkermans, T. J.; Falkowitz, D. M.; Trichonas, G., (**2024**). Chloroquine and hydroxychloroquine toxicity. In StatPearls. StatPearls Publishing.

[23] Sen, D.; Ghosh, T.; Dinda, B.; Chatterjee, T. K., Synthesis and antimalarial evaluation of some 4-quinazolinone derivatives based on febrifugine. *Journal of Advanced Pharmaceutical Technology & Research*, **2010**, *1*(4), 401-405. https://doi.org/10.4103/0110-5558.76439.

[24] Wang, L.; Bohmer, M. J.; Wang, J.; Nardella, F.; Calla, J.; Laureano De Souza, M.; Schindler, K. A.; Montejo, L.; Mittal, N.; Rocamora, F.; Treat, M.; Charlton, J. T.; Tumwebaze, P. K.; Rosenthal, P. J.; Cooper, R. A.; Chakrabarti, R.; Winzeler, E. A.; Chakrabarti, D.; Gray, N. S., Discovery of potent antimalarial type II kinase inhibitors with selectivity over human kinases. *Journal of Medicinal Chemistry*, **2024**, *67*(2), 1460-1480. https://doi.org/10.1021/acs.jmedchem.3c02046

[25] Kumar, S.; Bhardwaj, T. R.; Singh, R.; Sehgal, R., Drug targets for resistant malaria: Historic to future perspectives. *Biomedicine & Pharmacotherapy*, **2018**, *104*, 8-27. https://doi.org/10.1016/j.biopha.2018.05.009.

[26] Reyser, T.; Paloque, L.; Augereau, J. M.; Di Stefano, L.; Benoit-Vical, F., Epigenetic regulation as a therapeutic target in the malaria parasite *Plasmodium falciparum*.

Malaria Journal, **2024**, *23*(1), 44. https://doi.org/10.1186/s12936-024-04855-9

[27] Marques-da-Silva, C.; Schmidt-Silva, C.; Kurup, S. P., Hepatocytes and the art of killing Plasmodium softly. *Trends in Parasitology*, **2024**, *40*(6), 466-476. https://doi.org/10.1016/j.pt.2024.04.004.

[28] Hanau, S.; Helliwell, J. R., Glucose-6-phosphate dehydrogenase and its 3D structures from crystallography and electron cryo-microscopy. *Acta Crystallographica Section F*, **2024**, *80*(10), 236-251. https://doi.org/10.1107/S2053230X24008112.

[29] Katrib, M.; Ikin, R. J.; Brossier, F.; Robinson, M.; Slapetova, I.; Sharman, P. A.; Walker, R. A.; Belli, S. I.; Tomley, F. M.; Smith, N. C., Stage-specific expression of protease genes in the apicomplexan parasite *Eimeria tenella*. *BMC Genomics*, **2012**, *13*, 685. https://doi.org/10.1186/1471-2164-13-685.

[30] Rosenthal, P. J., Cysteine proteases of malaria parasites. *International Journal for Parasitology*, **2004**, *34*(13-14), 1489-1499. https://doi.org/10.1016/j.ijpara.2004.10.003.

[31] Rosenthal, P. J., Falcipain cysteine proteases of malaria parasites: An update. *Biochimica et Biophysica Acta (Proteins and Proteomics)*, **2020**, *1868*(3), 140362. https://doi.org/10.1016/j.bbapap.2020.140362.

[32] Melo, P. M. S.; El Chamy Maluf, S.; Azevedo, M. F.; Paschoalin, T.; Budu, A.; Bagnaresi, P.; Henrique-Silva, F.; Soares-Costa, A.; Gazarini, M. L.; Carmona, A. K., Inhibition of *Plasmodium falciparum* cysteine proteases by the sugarcane cystatin CaneCPI-4. *Parasitology International*, **2018**, *67*(2), 233-236. https://doi.org/10.1016/j.parint.2017.12.005.

[33] Ettari, R.; Previti, S.; Di Chio, C.; Zappalà, M., Falcipain-2 and Falcipain-3 inhibitors as promising antimalarial agents. *Current Medicinal Chemistry*, **2021**, *28*(15), 3010-3031. https://doi.org/10.2174/0929867327666200730215316.

[34] Ettari, R.; Bova, F.; Zappalà, M.; Grasso, S.; Micale, N., Falcipain-2 inhibitors. *Medical Research Reviews*, **2010**, *30*(1), 136-167. https://doi.org/10.1002/med.20163.

[35] Humphrey, W.; Dalke, A.; Schulten, K., VMD: Visual molecular dynamics. *Journal of Molecular Graphics*, **1996**, *14*(1), 33-38.

[36] Seeliger, D.; de Groot, B. L., Ligand docking and binding site analysis with PyMOL and AutoDock/Vina. *Journal of Computer-Aided Molecular Design*, **2010**, *24*(5), 417-422. https://doi.org/10.1007/s10822-010-9352-6.

[37] Berman, H. M.; Westbrook, J.; Feng, Z.; Gilliland, G.; Bhat, T. N.; Weissig, H.; Shindyalov, I. N.; Bourne, P. E., The Protein Data Bank. *Nucleic Acids Research*, **2000**, *28*(1), 235-242. https://doi.org/10.1093/nar/28.1.235.

[38] RDKit, (n.d.). https://www.rdkit.org/ (accessed August 14, **2025**).

[39] Lu, C.; Wu, C.; Ghoreishi, D.; Chen, W.; Wang, L.; Damm, W.; Ross, G. A.; Dahlgren, M. K.; Russell, E.; Von Bargen, C. D.; Abel, R.; Friesner, R. A.; Harder, E. D., OPLS4: Improving force field accuracy on challenging regimes of chemical space. *Journal of Chemical Theory and Computation*, **2021**, *17*(7), 4291-4300. https://doi.org/10.1021/acs.jctc.1c0030.

[40] Chatterjee, S.; Maity, A.; Chowdhury, S.; Islam, M. A.; Muttinini, R. K.; Sen, D., *In silico* analysis and identification of promising hits against 2019 novel coronavirus 3C-like main protease enzyme. *Journal of Biomolecular Structure and Dynamics*, **2021**, *39*(14), 5290-5303. https://doi.org/10.1080/07391102.2020.1787228.

[41] Eberhardt, J.; Santos-Martins, D.; Tillack, A. F.; Forli, S., AutoDock Vina 1.2.0: New docking methods, expanded force field, and Python bindings. *Journal of Chemical Information and Modeling*, **2021**, *61*(8), 3891-3898. https://doi.org/10.1021/acs.jcim.1c00203.

[42] Debnath, S.; Sen, D., Mushrooms are potential foods against cancer: Identified by molecular docking and molecular dynamics simulation. *Natural Product Research*, **2022**, *36*(10), 2604-2609. https://doi.org/10.1080/14786419.2021.1912041.

[43] Daina, A.; Michielin, O.; Zoete, V., SwissADME: A free web tool to evaluate pharmacokinetics, drug-likeness and medicinal chemistry friendliness of small molecules. *Scientific Reports*, **2017**, *7*, 42717. https://doi.org/10.1038/srep42717.